Geomagnetic variation anomalies in northern England: processing and presentation of data from a non-simultaneous array.

Geophysical J. R. astr. Soc. 1983, 75, 513-539.
DOI: 10.1111/j.1365-246X.1983.tb01938.x

D. Beamish Geomagnetism Unit, Institute of Geological Sciences, Murchison House, West Mains Road, Edinburgh EH9 3LA
R. J. Banks Department of Environmental Sciences, University of Lancaster, Lancaster LAI 4YQ

Summary. The block and basin structure of northern England has been investigated by an array of 35 magnetometer stations over a grid with a spacing of 10 km. Recordings at these sites were made simultaneously with those at a reference site. Using the common reference data, transfer function analysis enables the three anomalous field components to be estimated at each site, for the period range $10-10^4$ s. Using the transfer functions obtained, maps of the anomalous field components may be generated across the array, and used for interpretation of electrical conductivity structure. Maps thus obtained from the non-simultaneous array data in northern England are used to illustrate the advantages of the method, and provide evidence of an east–west current flow concentrated along the southern margin of the Northumberland Trough. The limitations of the procedure, although slight, are considered. The errors which arise in the method are deduced and techniques for their removal are suggested.

Introduction

The process of electromagnetic induction in the Earth provides internal fields (both normal and anomalous) which, when estimated, can be used to infer electrical conductivity structure. Maxwell's equations, which govern the process, are both solved and understood as a boundary value problem. The boundary values taken in relation to a given problem may be local, regional or global. For many of the variation fields covering the period range $10-10^4$ s, a *complete* description of the process is achieved only through a definition of the globally bounded field values. In many cases it has become apparent that a number of local field relationships obtained from induction studies can only be interpreted when consideration is given to the wider problem (e.g. Banks 1981).

Geomagnetic variational sounding, commonly referred to as geomagnetic deep sounding (GDS), uses geomagnetic variation measurements at discrete points over the Earth's surface to provide information about the conductivity structure. The area of the Earth's surface

covered by a GDS experiment will be relatively small, being limited by the number of magnetometers in relation to the site separations. If an experiment on upper-crustal (i.e. local) structure is to be undertaken, the typical site separation should be no greater than 20 km. With such a distance fixed, the regional coverage of the experiment will be governed by the number of magnetometers. When considering variation fields in the period range $10-10^4$ s it is possible to identify, from the literature, two main types of GDS experiment which have been used to investigate conductivity structure. The two types of experiment give rise to two different types of data which are used for analysis and interpretation:

(a) Single-site, or small number of sites, operated at a given time. The instrument(s) is moved to provide regional coverage. The output from such an experiment can be considered the single-site transfer function, or its equivalent (Everett & Hyndman 1967).

(b) Multiple-site, or array, operation. Such experiments have used 20–40 simultaneously recording instruments to provide local and regional coverage (Reitzel *et al.* 1970). The output from such an experiment is often an amplitude and phase map of the Fourier transforms of chosen events across the array.

The two types of experiment have both advantages and disadvantages in relation to the data provided and the assumptions made in the analysis and interpretation of the data (Beamish 1977). In defining upper crustal structure, from both types of experiment, we once again refer to the necessity for providing a regional coverage from small site separations in order to avoid spatial aliasing of local structure and in order to provide adequate regional boundary conditions. We suggest that a common reference site, used in conjunction with the former type of experiment, can resolve most (but not all) of the difficulties inherent in the two approaches. The limiting experimental requirement is for two magnetometers, one fixed (the reference site) and one mobile (operating at a particular field site). The experimental procedure is obviously enhanced by increasing the number of field magnetometers operating at any one time. Regional, i.e. array-type, coverage is provided by moving the field magnetometer(s) when sufficient data have been obtained from each field site. Analysis of the data collected proceeds using the simultaneous data collected at each array site and the reference site. The use of reference field data to investigate conductivity structure is by no means new (Duffus *et al.* 1959) and the formalism by which such data may be processed and analysed has been stated (Schmucker 1970). However, only a very limited number of analyses have appeared which have fully exploited the advantages of such an approach.

We have utilized the above experimental procedure to obtain geomagnetic variation data from northern England in order to study the conductivity structure of the region. The crustal structure for this region appears well-defined both geologically and geophysically. Site separations were of the order of 10 km and data were obtained from 38 sites across the area to provide regional coverage. Transfer function analysis was used to obtain estimates of the three anomalous field components at each array site, for the period range $10-10^4$ s. Such a uniform set of transfer functions can be used to predict and map the three anomalous field components associated with a particular horizontal variation field at the reference site. The technique is thus an extended form of hypothetical event analysis introduced by Bailey *et al.* (1974). As with most other array experiments, the limitation of the procedure is that the normal field remains undefined. We would like to assume that the maps generated by hypothetical event analysis represent anomalous fields due to internal currents which flow in response to a specified normal field across the region. Under this assumption, which corresponds to a real physical process, the boundary conditions would be provided in the specification of the normal field. In obtaining transfer function estimates in relation to a reference site and then using hypothetical event analysis to map the anomalous field, we merely approximate such a process.

This paper illustrates the advantages of using a common reference site in terms of the additional information that is generated. The limitations of the procedure which arise from a bias introduced by anomalous horizontal fields at the reference sites are considered and techniques for the removal of such bias are suggested.

Crustal structure of the array area

The site coverage, in relation to the main geological and structural units of northern England, is shown in Fig. 1. The region was chosen because it represents an area that is geologically well-known and across which the upper crustal structure has been well-investigated geophysically. The most important event in the post-Caledonian geology of northern England was the emplacement of granite batholiths during the lower Devonian. The array is

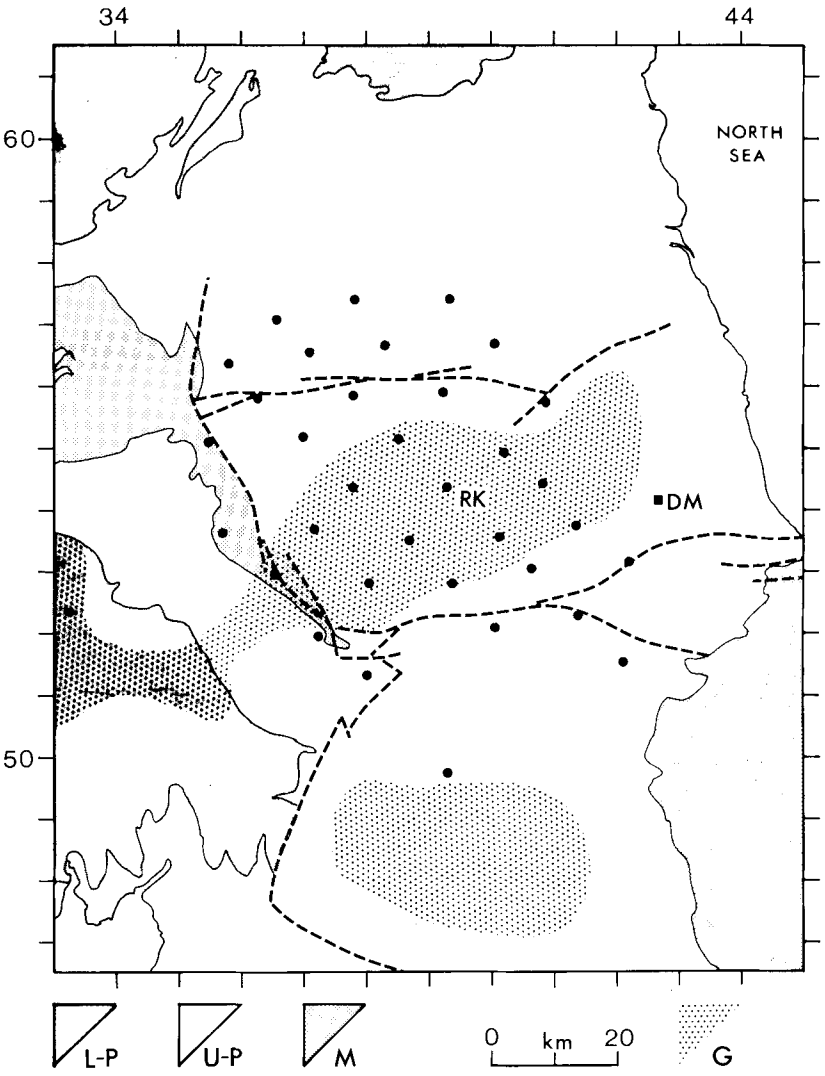

Figure 1. Map of northern England showing the 34 field fluxgate sites and the reference site of Durham (DM). Major regional faults are indicated by broken lines. The site of Rookehope (RK) is centrally located within the Alston Block. The major geological units outlined are, L–P: Lower Palaeozoic, U–P: Upper Palaeozoic, M: Mesozoic, G refers to the inferred distribution of granite batholiths across the region.

centred on the Weardale granite whose outline is deduced from detailed gravity surveys (Bott 1967) and which lies concealed beneath Carboniferous strata. The granite surface is considered non-uniform and comprises five cupolas as defined by the Bouger anomaly map (Bott 1967). A second, contemporaneous batholith (the Wensleydale granite) underlies the Askrigg block in the south of the array area.

The concealed, low density Weardale granite is thought to have maintained the Alston block as a single, stable structural unit and topographic 'high' during the lower Carboniferous. Consequently, sedimentation was greatest in basins to the north (Northumberland basin) and south (Stainmore basin) of the block and separated from it by east–west-trending, hinge-line faults. The Weardale granite appears to form the eastern end of a largely unexposed and possibly continuous belt of granite which underlies the Lake District, to the west (Bott 1974). The north–south-trending Pennine faults, defining the western margin of the Alston block and the eastern margin of the Carboniferous/Permo-Triassic sedimentary basin of the Vale of Eden, possess a more complex structural history. They appear to have been initiated during the Hercynian movements along what may have been an earlier line of weakness bordering the western margin of the Weardale granite (Bott 1967, 1974). The Carboniferous rocks dominate the surface outcrop. Substantial lateral variations occur in the thickness of the sedimentary cover and are most acute over the fault-bounded margins of the Alston block. The greatest thickness occurs across the Northumberland Trough (3.5 km) and in the Stainmore Trough (2.5 km) while, on average, less than 1 km appears above the block (Bott 1967; Swinburn 1975). Gravitationally and magnetically, the basement beneath the sedimentary basins appears to be featureless. The suggested upper crustal structure is a thick (10–15 km) pile of lower Palaeozoic greywackes (*P*-wave velocity from 5.5 to 6.0 km s^{-1}, Swinburn 1975) through which the granites have been intruded. Seismic data (Swinburn 1975) suggest that the lower crust extends from a depth of about 12 km to the Mohorovičić discontinuity at a depth of about 27 km. The *P*-wave velocity at the top of the lower crust is about 6.5 km s^{-1} and may increase gradually with depth.

The region is distinguished geophysically by high heat flow values in relation to the average heat flow of mainland Britain. One of the two 'belts' of high heat flow values identified by Richardson & Oxburgh (1979) traverses the region from the south-east to the north-west. It has been argued, on the basis of a more detailed examination of heat flow values from north-east England (England, Oxburgh & Richardson 1980), that differences in the thermal regimes of the high heat-producing granites beneath the Alston and Askrigg blocks can be accounted for by geochemical differences, within each granite, extending to depths of 15 km or more.

In summary, all the geological and geophysical studies of the region point towards a relatively straightforward upper crustal structure. The most important lower Palaeozoic basement feature is the Weardale granite which has been modelled as a uniform, low-density granite possibly extending to mid-crustal depths, and whose outline is given in Fig. 1. The Alston block, which overlies the granite, is fault-bounded on three sides which separate two major Carboniferous sedimentary basins to the north and south and a Carboniferous/permo-Triassic sedimentary basin to the west. One of the aims of the present investigation is to use the well-established block and basin characteristics of the region together with the spatial control provided by the array sites to examine the resolution afforded by the GDS technique.

Transfer functions from non-simultaneous array operation

The formalism by which geomagnetic array data may be processed to obtain transfer functions relating to geoelectric structure was developed by Schmucker (1964), Everett &

Hydnman (1967) and described in detail by Schmucker (1970, 1973). The assumption of a quasi-uniform external field permits the concept of linear transfer functions between field components as functions of frequency at one or more observation points. We write

$$\begin{pmatrix} H_a \\ D_a \\ Z_a \end{pmatrix} = \begin{pmatrix} h_H & h_D & h_Z \\ d_H & d_D & d_Z \\ z_H & z_D & z_Z \end{pmatrix} \begin{pmatrix} H_n \\ D_n \\ Z_n \end{pmatrix} + \begin{pmatrix} \epsilon_H \\ \epsilon_D \\ \epsilon_Z \end{pmatrix} \tag{1}$$

where all quantities are complex and functions of frequency. The subscripts a and n refer to the anomalous and normal parts of the observed variation field (H, D, Z) respectively. The vector (ϵ_H, ϵ_D, ϵ_Z) is an error term which is to be minimized in the determination of the transfer function matrix.

The data set, available over N records, will contain a distribution of quasi-uniform external fields described by their associated wavenumbers k_I, $I = 1, N$. Both the value and variance of the mean value of the population is a function of geomagnetic latitude and the frequency of the variation field (e.g. Banks 1981). At the latitude of the present study, the data analysis techniques used ensure that, at best, k varies in a statistically random manner over the available data set or, at worst, that the bias introduced by a population with small variance (in k) is minimized (Beamish 1979). We may then set $Z_n = 0$. Ideally the relationships described by (1) relate three anomalous field components (H_a, D_a, Z_a) to the three normal field components (H_n, D_n, 0). The problem, in practice, is the separation of the three field components observed at one or more sites, into anomalous and normal parts. In the first instance, the three components (H_i, D_i, Z_i) observed at each site (i) may be used to obtain the single-site vertical field transfer function (t_H, t_D) according to

$$Z_i = t_{Hi} \cdot H_i + t_{Di} \cdot D_i + \epsilon_Z \tag{2}$$

where (t_{Hi}, t_{Di}) denote the values of (t_H, t_D) at site i. If $Z_n = 0$, then the transfer function (t_H, t_D) can only be considered a valid approximation to the required vertical field transfer function (z_H, z_D) if the observed horizontal fields ($H = H_a + H_n$, $D = D_a + D_n$) may be approximated by (H_n, D_n), i.e. we require the anomalous to observed field ratios H_a/H and D_a/D to be small. If the single-site transfer function is to be used for array application (i.e. for spatial mapping of the anomalous vertical field) it can be seen that its main disadvantage is that the relationship neglects the spatial variation in the anomalous horizontal field across the array. Common reference processing can overcome this difficulty as described below.

The method of site deployment for the array experiment described in this paper ensured simultaneous records between each array site and a common reference. A reference site could be chosen on the basis of the spatial gradients of the anomalous field components across the region. The reference site could then be located in a region associated with the smallest gradients. Obviously such a method presupposes the anomalous fields are known. In practice a reference site is chosen on the basis of *known* conductive structures and is located away from such structures as is practical. The distance between the array sites and the reference should not exceed a typical scale length of the external inducing field. In our case the reference site was located on the eastern margin of the array and on the Alston Block, i.e. away from the two east–west-trending sedimentary basins, lying to the north and south.

It is arguable whether, for an array of the present dimensions, the normal field can be defined (Beamish 1983). Inevitably, in the first instance, a determination of the transfer functions proceeds using the fields common to each array site (H_i, D_i, Z_i) and the reference site (H_r, D_r, Z_r). Using such common reference processing, two sets of equivalent transfer functions may be obtained. In the first case, the anomalous field components of (1) are

estimated by difference fields as:

$$\Delta H_i = H_i - H_r = h_{Hi} \cdot H_r + h_{Di} \cdot D_r + \epsilon_{Hi} \tag{3}$$

$$\Delta D_i = D_i - D_r = d_{Hi} \cdot H_r + d_{Di} \cdot D_r + \epsilon_{Di} \tag{4}$$

$$\Delta Z_i = Z_i - Z_r = z_{Hi} \cdot H_r + z_{Di} \cdot D_r + \epsilon_{Zi} \tag{5}$$

where the transfer functions with the subscript of i indicate estimated values. In the second case, transfer functions may be obtained using the observed field at each site together with the observed horizontal field at the reference site as:

$$H_i = h'_{Hi} \cdot H_r + h'_{Di} \cdot D_r + \epsilon'_{Hi} \tag{6}$$

$$D_i = d'_{Hi} \cdot H_r + d'_{Di} \cdot D_r + \epsilon'_{Di} \tag{7}$$

$$Z_i = s_{Hi} \cdot H_r + s_{Di} \cdot D_r + \epsilon'_{Zi}. \tag{8}$$

It is evident that simple identities must exist between the transfer functions defined by equations (3)–(5) and those defined by equations (6)–(8). For the case of the horizontal field transfer functions we obtain, $h'_{Hi} = h_{Hi} + (1, 0)$, $h'_{Di} = h_{Di}$, $d'_{Hi} = d_{Hi}$ and $d'_{Di} = d_{Di} + (1, 0)$. For the case of the vertical field transfer functions, we must first define the single-site vertical field transfer function at the reference site, i.e.

$$Z_r = t_{Hr} \cdot H_r + t_{Dr} \cdot D_r + \epsilon_{Zr} \tag{9}$$

to obtain the identities, $s_{Hi} = z_{Hi} + t_{Hr}$ and $s_{Di} = z_{Di} + t_{Dr}$.

In defining the estimated transfer function matrix given by equations (3)–(5), we have made no attempt to estimate the normal field quantities required by equation (1). The estimated transfer function matrix merely defines those transfer functions, which may be obtained in practice at each array site, using common reference processing.

Determination of the transfer functions

The data available for analysis come from the array of 38 fluxgate magnetometers covering the Alston Block of northern England (Fig. 1). Site separations were of the order of 10 km. Of the 38 sites operated, 35 provided sufficient quantities of valid data for analysis. Six field fluxgates were operated simultaneously with the continuously recording reference site at Durham (DM) employing a low-noise rubidium vapour magnetometer. Field components sampled at 10 s (fluxgate) and 2.5 s (rubidium) were recorded digitally on cassettes. Instrumental clocks were synchronized every 3–4 days, at each cassette change, and provided a relative time drift of less than ± 5 s over this period. The bandwidth available for analysis is necessarily limited. The high-frequency limit is governed by the longest sampling interval used which is usually a function of magnetometer sensitivity. For this data set, the Nyquist period is 20 s. The low-frequency limit is governed by the low-frequency stability of the magnetometer systems together with source field effects. Since temperature corrections were applied to the field fluxgate data, the limiting factor is the source field effects. Since our analysis requires source field variability we restrict our attention to the variation periods not influenced by the daily variation field. On this basis our analysis would be restricted to variation periods of less than 3 hr. In practice our analysis is further restricted by a requirement for a sufficient number of degrees of freedom, to variation periods of less than 2 hr (7200 s).

To provide results over the three decades $10–10^4$ s, data decimation or averaging is required. Two sets of data files (A and B) were made available for analysis at each site. The A files consisted of 12 hr of 60 s (averaged) data and the B files consisted of 2 hr of 10 s

Table 1. The period band scheme used in the analysis. ND refers to the number of real degrees of freedom of each band obtained from each file (see text).

Band	Period(s)	ND
1	7200–4000	32
2	5000–3000	32
3	4000–2000	64
4	3000–1000	64
5	2000–900	64
6	1500–800	98
7	1000–600	128
8	600–400	128
9	500–300	128
10	400–200	64
11	250–150	64
12	200–90	128
13	100–70	128
14	80–60	128
15	70–50	128
16	60–40	256
17	50–30	256
18	40–20	512

data. Each complete day of data thus provided two A and 12 B files. The subsequent analysis is based on between 5 and 15 complete days of selected data at each site. The transfer function estimates are required as functions of frequency. Spectral analysis is carried out on each file (A and B) using complex demodulation (Banks 1975) to provide band-averaged spectral quantities. The period range $10–10^4$s was divided logarithmically into 18 overlapping period bands. Nine long-period bands were obtained from each A file and nine short-period bands from each B file. The degrees of freedom provided by the 18 band scheme (Table 1) were found to provide the required combination of stability and resolution in the transfer functions obtained.

As indicated by equations (3)–(5), the estimates of the transfer function matrix are obtained as three uncoupled equations. Equations (2)–(9) all then represent two input/one output linear relationships between the spectral quantities. As indicated in these equations, the least-squares estimator which minimizes noise on the output channel is used to obtain each transfer function pair. The two reference horizontal components which appear as the input channels in (3)–(5) and (6)–(8) are recorded by a low-noise rubidium vapour magnetometer. These channels provide an improvement in signal to noise ratio of the order of 100 when compared to the output channels which are obtained from the field fluxgate magnetometers. The expressions which minimize the noise on the output channels are considered the more appropriate in the present case. A requirement that bias errors, due to different noise contributions on all three data channels, be assessed is not necessary if the bias error can be reduced to a value less than or equal to the random error associated with the estimate. This can be achieved if a high (> 0.95) normalized multiple coherence (White 1973) is associated with each determination. This is generally the case for the data under consideration.

Each file (A and B) was used to obtain an estimate of the transfer function in the above manner. The random error associated with the determination was estimated using the unit vector approach of Everett & Hyndman (1967); the demodulates within each spectral band being arranged to be statistically independent. Given N such determinations of the real part

(C_R) of a transfer function C, a final weighted mean estimate ($\hat{C}_R$) of the real part of the transfer function together with its associated standard error $\hat{\sigma}_R$ is obtained as:

$$\hat{C}_R = \frac{\sum_{i=1}^{N} w_i C_{Ri}}{\sum_{i=1}^{N} w_i}$$

$$\hat{\sigma}_R^2 = \frac{1}{\sum_{i=1}^{N} w_i}$$

where the weighting function is $w_i = 1/\sigma_i^2$, σ_i being the standard error associated with each individual determination of C_{Ri}. The subcript i refers to an individual determination of a transfer function from an A or B file. Typically, based on 10 days data, $N_A = 2 \times 10 = 20$ and $N_B = 12 \times 10 = 120$. The variance of the weighted mean, estimated in this way, provides the smallest standard error of any linear least-squares method. An equivalent procedure also provides a weighted mean estimate ($\hat{C}_I$) of the imaginary part of the transfer function $\hat{C}$ together with its associated weighted standard error $\hat{\sigma}_I$. The final standard error ($\hat{\sigma}_c$) associated with $\hat{C}$ is then given by

$$\sigma_c^2 = \sigma_R^2 + \sigma_I^2 .$$

Frequency dependence of the transfer functions

Estimates of the three components of the anomalous field at each array site have been obtained in terms of the transfer function matrix for the period range $10-10^4$s. Let ΔH, ΔD and ΔZ denote the estimates of the anomalous field obtained from the transfer functions (h_H, h_D), (d_H, d_D) and (z_H, z_D), respectively. A further estimate of the anomalous vertical field is obtained from the transfer function (s_H, s_D); we denote this estimate as S. In addition to the transfer functions obtained using common reference processing, a further estimate of the anomalous vertical field is obtained from the single-site transfer function (t_H, t_A); we denote this estimate as T. We begin by considering the frequency dependence of the vertical field transfer function estimates T, S and ΔZ. In all three cases, induction arrows (Schmucker 1970) allow the complex transfer function (X, Y) to be presented in terms of a magnitude and azimuth which defines the strike direction of structure. We here define real (R) and imaginary (I) induction arrows to have magnitudes:

$$G_R = \{[\mathrm{Re}(X)]^2 + [R_e(Y)]^2\}$$

$$G_I = \{[\mathrm{Im}(X)]^2 + [\mathrm{Im}(Y)]^2\}$$

with corresponding azimuths:

$$\theta_R = \tan^{-1} - [\mathrm{Re}(Y)/\mathrm{Re}(X)]$$

$$\theta_I = \tan^{-1} - [\mathrm{Im}(Y)/\mathrm{Im}(X)].$$

Defined clockwise from geomagnetic north. Declination varies by less than 1° over the array region.

We first consider the induction arrows determined from the transfer function denoted by T at the reference site of DM; these are shown in Fig. 2. If the reference site were normal, both C_R and C_I would approach zero and both θ_R and θ_I would be undefined. The referenced site, quite clearly, cannot be regarded as normal. In fact certain features apparent

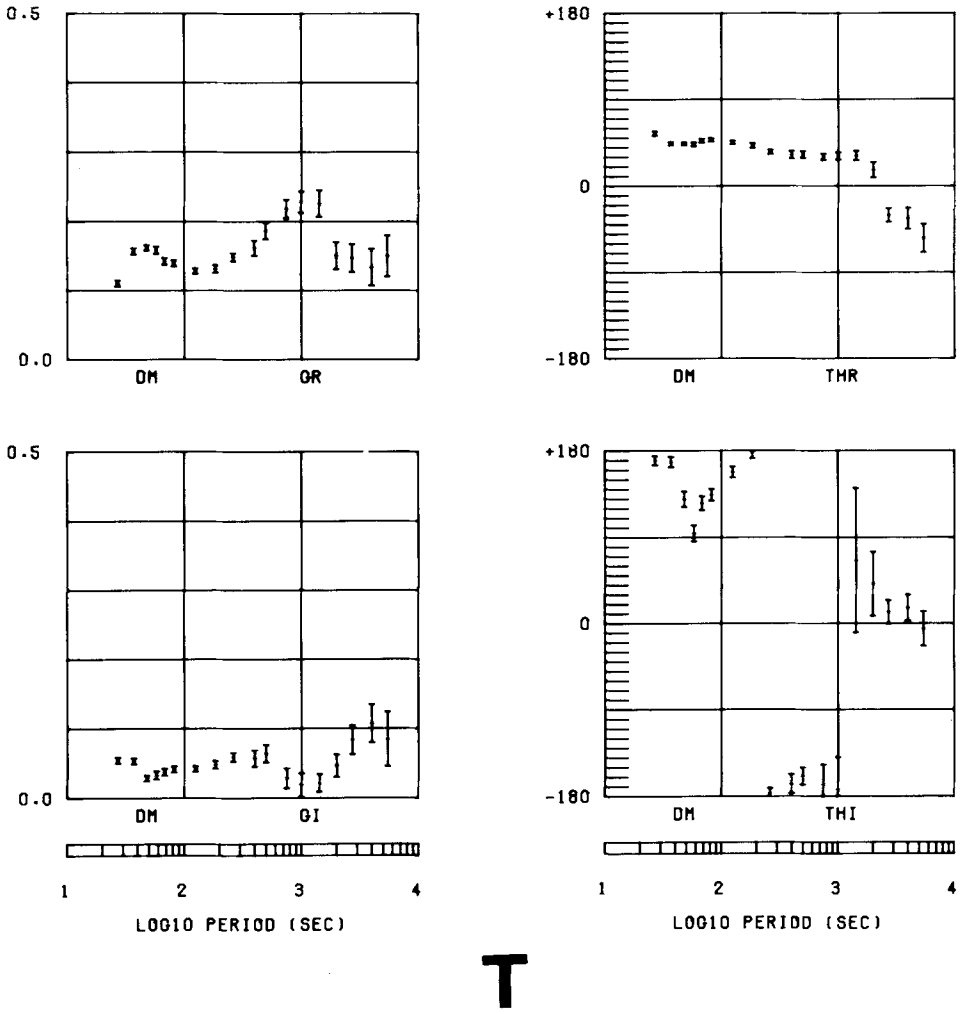

Figure 2. Induction arrows obtained from the T transfer function estimate at the reference site of DM. GR, THR are the magnitude and azimuth of the real arrow, respectively. GI, THI are the magnitude and azimuth of the imaginary arrow, respectively. Error bars are ±1 sd (68 per cent confidence limits).

in Fig. 2 are consistent with features noted in single-site transfer functions available over a much wider area of Britain. Banks & Beamish (1983) have indicated three different frequency ranges that correspond to three different modes of induction that influence the anomalous vertical fields determined by the T transfer function:

(a) At period > 2000 s, the real induction arrows point westward indicating the influence of induced current flow in the deep Atlantic Ocean.

(b) At periods < 2000 s, the anomalous vertical field is, at many sites, produced by the perturbation of currents driven through the land as part of a thin-sheet induction process which includes the shelf seas and major sedimentary basins.

(c) At periods < 100 s, local induction in isolated conductive structures may become the more important mechanism.

The reference site of DM is less than 20 km from the North Sea yet the anomalous vertical field at the longest periods results from the direct effect of currents in the Atlantic

Ocean. At periods < 2000 s the real arrow rotates under the influence of currents induced in the North Sea and in the N–S orientated sedimentary basins of eastern England and the North Sea. At periods < 2000 s we observed two peaks in the magnitude of the anomalous vertical field. The maximum anomalous vertical field occurs at a period of 1000 s and is largely in-phase (i.e. real). A secondary maximum occurs at much shorter periods (50 s).

We next consider the induction arrows determined from the transfer functions T, S and ΔZ at a site (RK) some 34 km to the west of the reference site of DM and chosen because of its central position with regard to both the array area and the Alston Block (Fig. 1). The induction arrows determined from estimate T are shown in Fig. 3. We note that at the longest periods the results obtained are very similar to those at DM (Fig. 2). At periods < 2000 s we again note that $|G|$ displays both long- (750 s) and short- (60 s) period maxima. In contrast to the longer-period response, the response at short periods at this site displays very different characteristics, in terms of both G_R, θ_R and G_I, θ_I, to those observed at the reference site of DM. We conclude that the response at short periods is determined largely by local structure.

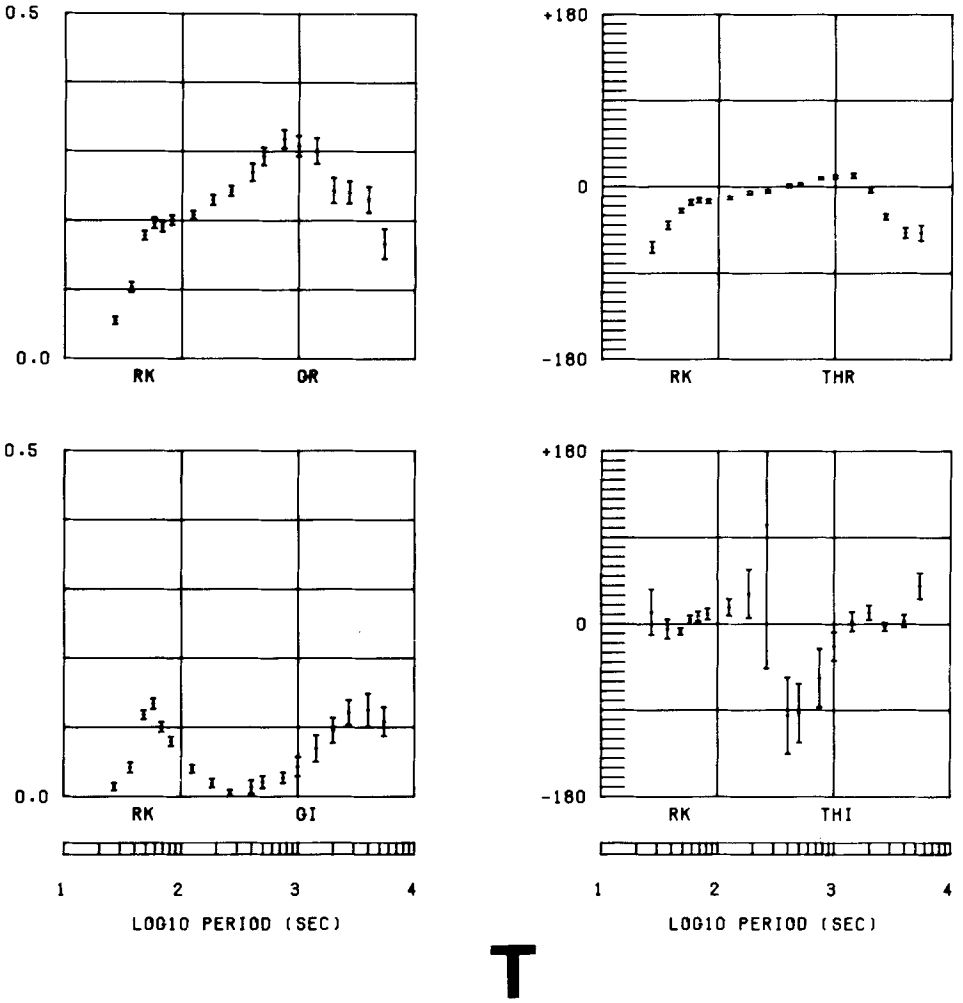

Figure 3. Induction arrows obtained from the T transfer function at RK, and as for Fig. 2.

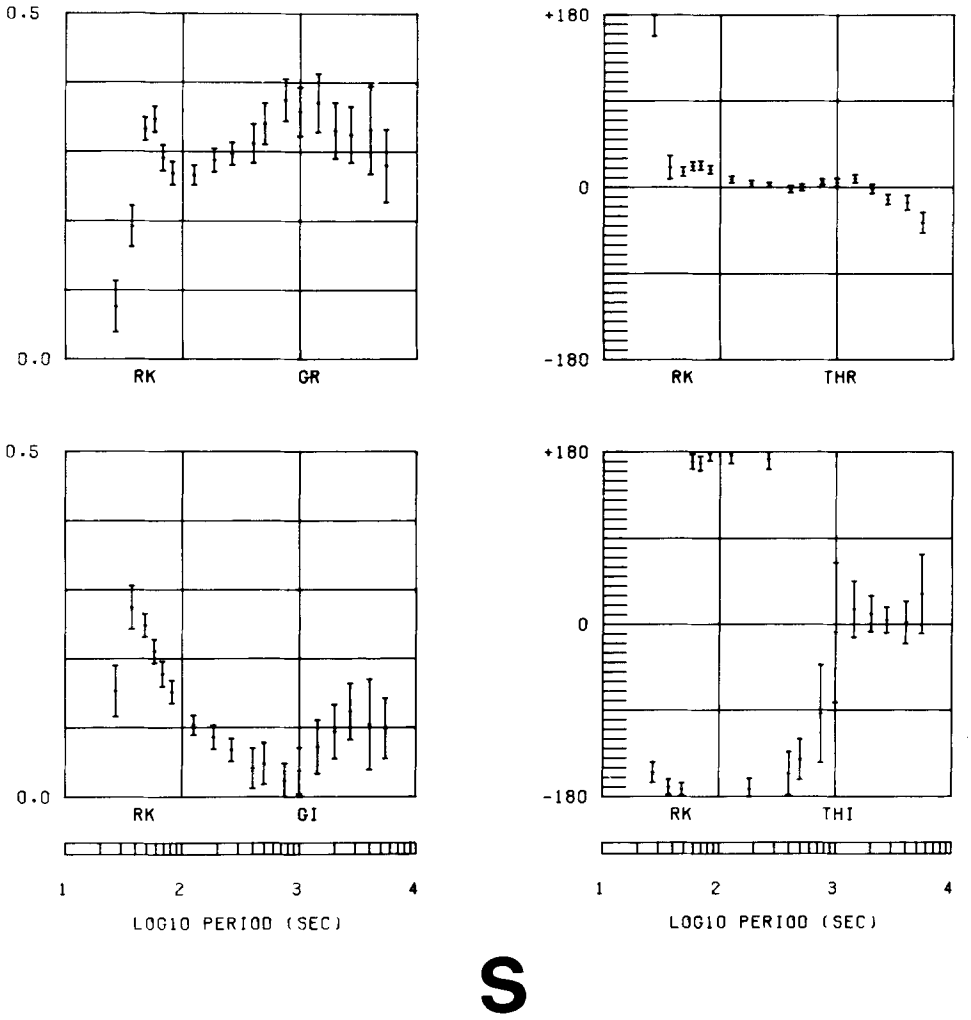

Figure 4. Induction arrows obtained from the S transfer function at RK, and as for Fig. 2.

The induction arrows determined from the T transfer function may now be compared with the induction arrows determined from the S transfer function which are shown in Fig. 4. The larger errors bars obtained for the S result are due to the reduced amount of data analysed. We note, from the definitions of the transfer functions, that any significant differences between the two determinations are due to the differences in horizontal fields recorded at the two sites. Comparing Figs 3 and 4, we observe that although the form of the vertical field response has not changed, the magnitude of both real and imaginary parts is significantly different between the two determinations. We observe that the magnitude of the anomalous vertical field as estimated by S is significantly larger than that estimated by T over the three decades. The difference is most pronounced at periods <100 s. We conclude that the T transfer function at RK is significantly downward-biased by the presence of anomalous horizontal fields.

The third vertical field transfer function estimate we consider at RK is denoted as ΔZ. This relates the difference in vertical fields between RK and DM (the reference) to the

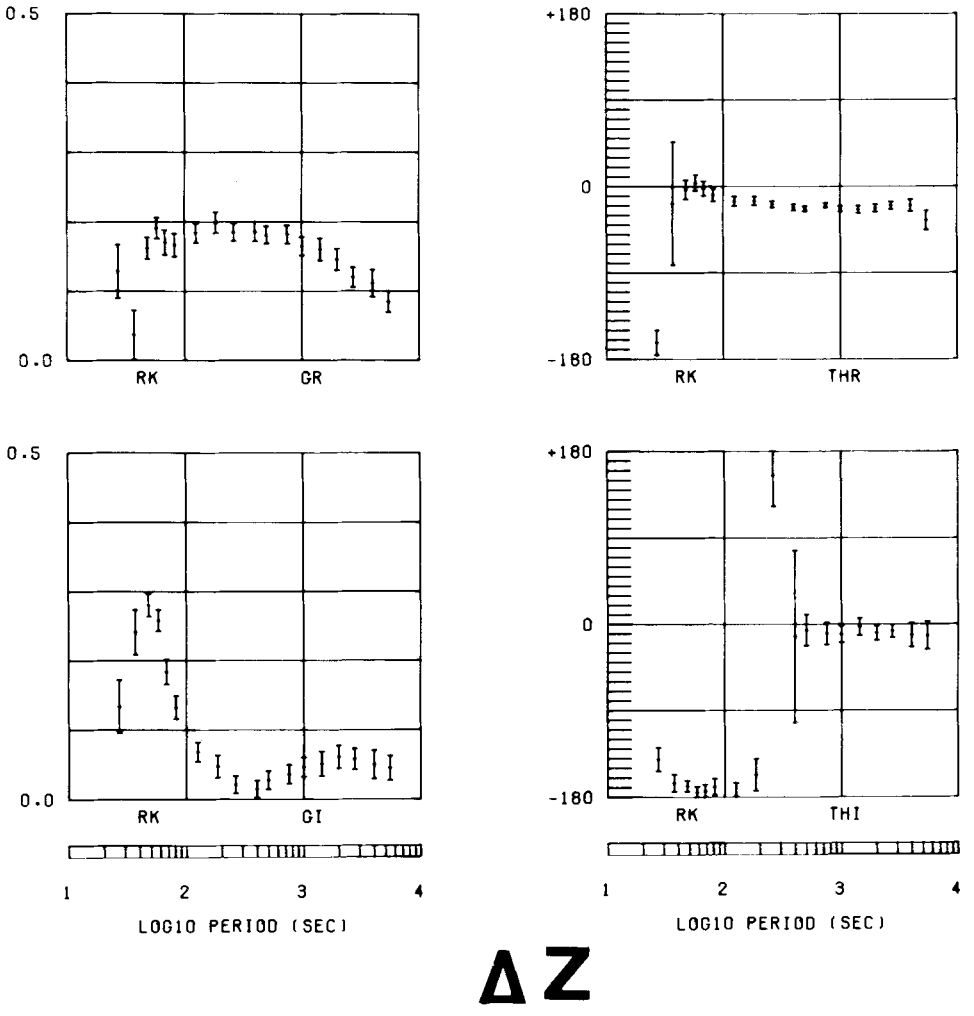

Figure 5. Induction arrows obtained from the ΔZ transfer function at RK, and as for Fig. 2.

reference horizontal fields. The induction arrows obtained from the transfer function ΔZ are shown in Fig. 5 and are significantly determined over the three decades. It is apparent that significant differences exist in both the real and imaginary parts of the anomalous vertical fields at the two sites. The largest difference occurs at short periods (60 s) in the imaginary part.

We now consider the frequency dependence of the anomalous horizontal fields ΔH and ΔD obtained at the same site using common reference processing. The horizontal field transfer

$$\begin{pmatrix} h_H & h_D \\ d_H & d_D \end{pmatrix}$$

from which we can obtain a further independent measure of the strike direction of conductivity structure (Schmucker 1970). The strike direction is obtained by combining the transfer functions relating to both ΔH and ΔD and we prefer, in the first instance, to

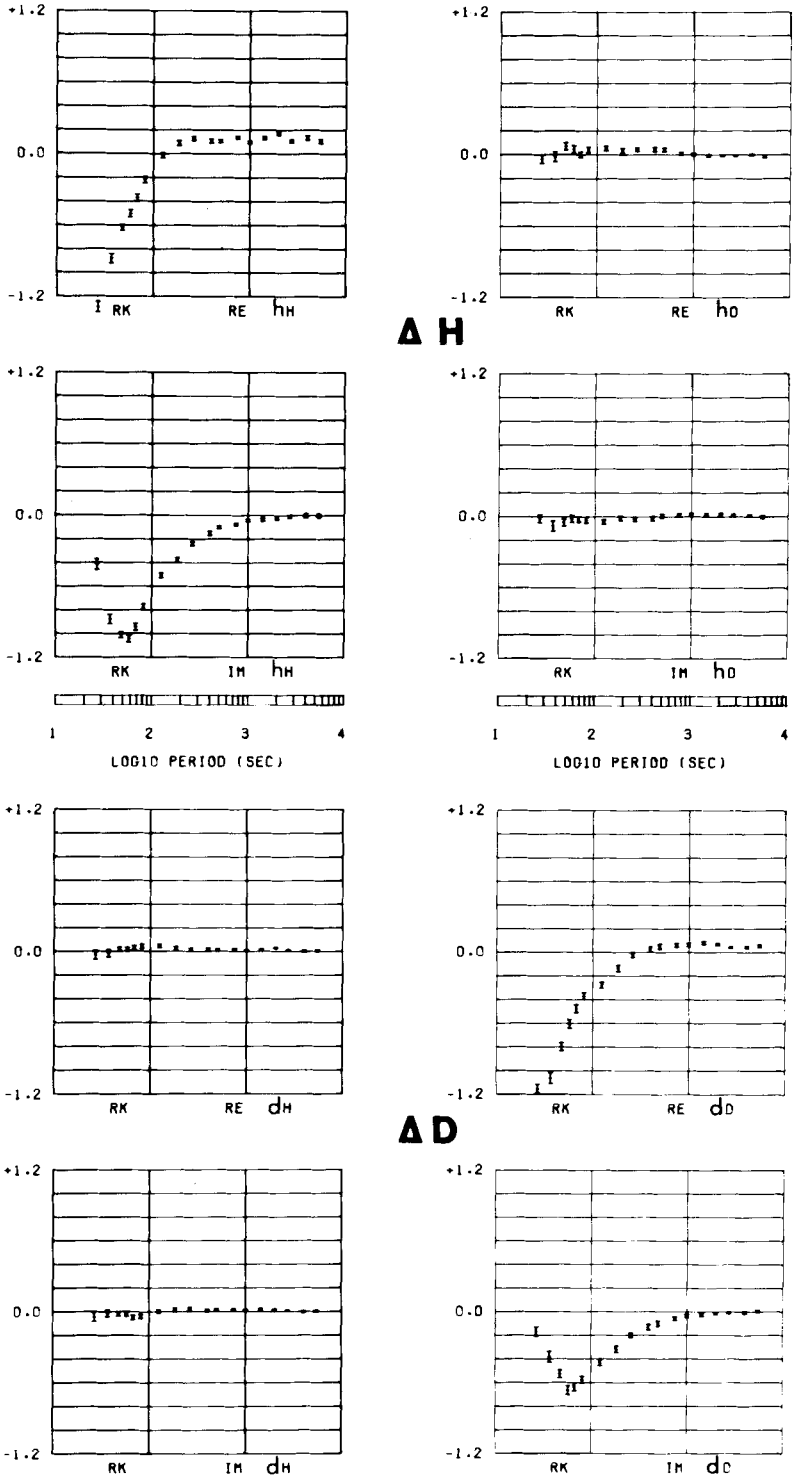

Figure 6. The real (RE) and imaginary (IM) parts of the ΔH (h_H, h_D) and ΔD (d_H, d_D) transfer functions ar RK. Error bars are ±1 sd (68 per cent confidence limits).

consider the two anomalous field components separately. The transfer functions (h_H, h_D) relating to ΔH and (d_H, d_D) relating to ΔD are shown in Fig. 6. To a large extent, the horizontal field transfer functions observed at this site are typical of many sites in northern England. At periods >300 s, we find that the horizontal field differences in both H and D components are less than 20 per cent of the reference field components. The difference is largely confined to the real part. At long periods the horizontal fields at RK are greater than those at the reference site. At short periods (<100 s) the horizontal field differences approach the same magnitude as the reference field components due to a reduction in the horizontal fields at RK. The dominance of the diagonal elements of the horizontal field sub-matrix at short periods suggests that the anomalous horizontal field is produced by internal current flow possessing both N–S and E–W components.

Even with the limited amount of data presented, it is apparent that the well-resolved transfer function estimates, relating to both the vertical and horizontal anomalous fields, have gone some way towards the identification of two modes of induced current flow across the region. At periods <2000 s, a bimodal response is observed in the anomalous field components. At periods of about 1000 s, a maximum anomalous vertical field is observed which is largely in-phase with the reference horizontal fields. At this same period, the anomalous horizontal field is small and again largely in-phase with the reference horizontal fields. At periods around 60 s, a second maximum occurs in the anomalous vertical field whose magnitude is reduced with respect to the longer period maximum. At this same period, the anomalous horizontal field is substantial and approaches the same order of magnitude as the reference horizontal fields. Both vertical and horizontal anomalous fields at this period can display a substantial phase rotation with respect to the reference horizontal field.

Maps of the anomalous field components

The transfer functions obtained by common reference processing (equations 3, 4 and 5) provide estimates of the anomalous fields ΔH_i, ΔD_i, ΔZ_i at each array site (i), in relation to the horizontal fields recorded at the reference site. A second estimate of the anomalous vertical field, in relation to the reference horizontal fields, is obtained using equation (8) and is denoted by S_i. A third, more common, estimate of the anomalous vertical field is obtained using equation (2) from the field components at a single site and is denoted by T_i.

Several different approaches can be made in order to map the spatial behaviour of the transfer functions across the array. One such approach using vectors or arrows (Schmucker 1970) presents difficulties in interpretation when the conductivity structure is three-dimensional. We have found it preferable instead to use the transfer functions to predict and then map the anomalous field components across the array. Maps of the anomalous field components are generated by using the transfer functions to predict the anomalous fields ΔH, ΔD, ΔZ and S associated with a particular horizontal field (H_r, D_r) at the reference site. The technique is thus an extended form of hypothetical event analysis (HEA) introduced by Bailey *et al.* (1974). The technique has also been applied to the single-site estimates of the anomalous vertical field (T) under the assumption that both horizontal components are uniform across the array region. This assumption can be readily examined for the present region by mapping the anomalous horizontal fields ΔH and ΔD. We can also use the three anomalous vertical field estimates, T, S and ΔZ to examine the differences that result in the application of HEA to the three different estimates of the anomalous vertical field across the array region.

The most straightforward method of application of HEA is to consider a horizontal field at the reference site which is linearly polarized at azimuth θ and which has unit amplitude

and zero phase. Prior to any definition of an optimum phase of the anomalous field components, the real and imaginary parts of the fields are interpolated on to a regular grid for subsequent contouring. We here use a 5 km regular grid interval. The azimuth of the reference horizontal field is then varied to obtain the anomalous fields that define the conductivity structure in an optimum manner. The anomalous fields will maximize when the *local* current flow defines an E-polarization mode, i.e. when the local current flow is parallel to geoelectric strike. The transfer function estimates obtained are smooth functions of frequency and for the purposes of presentation we restrict ourselves to two frequency ranges that represent two distinct modes of induced current flow. We use the transfer function estimates for BAND 7 (1000–600 s) to represent the fields that are produced by the perturbation of currents driven through the land as part of a thin-sheet induction process. We use the estimates for BAND 15 (70–50 s) to represent the fields that are produced by local induction in isolated regions of high conductivity. The region across which the maps are presented is shown in Fig. 7. The contour maps are restricted to those regions that are well-defined by the array site coverage.

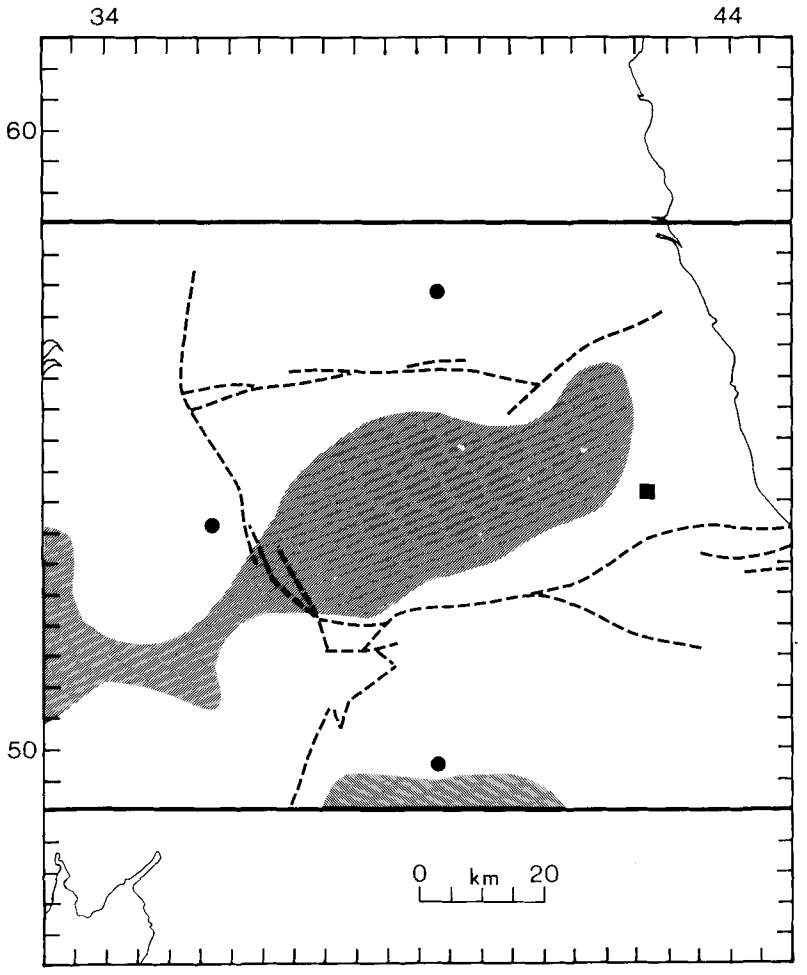

Figure 7. Reference map for contour plots of anomalous field components. Solid horizontal lines denote N–S extent of contoured region. Position of four extreme array sites are given for reference.

Prior to the spatial mapping of the anomalous field components using HEA, the behaviour of the fields as a function of the azimuth (θ) of the reference horizontal field can be examined. In Fig. 8(a), the behaviour of the real and imaginary parts of the anomalous field components ΔH, ΔD and ΔZ is plotted as a function of the reference horizontal field

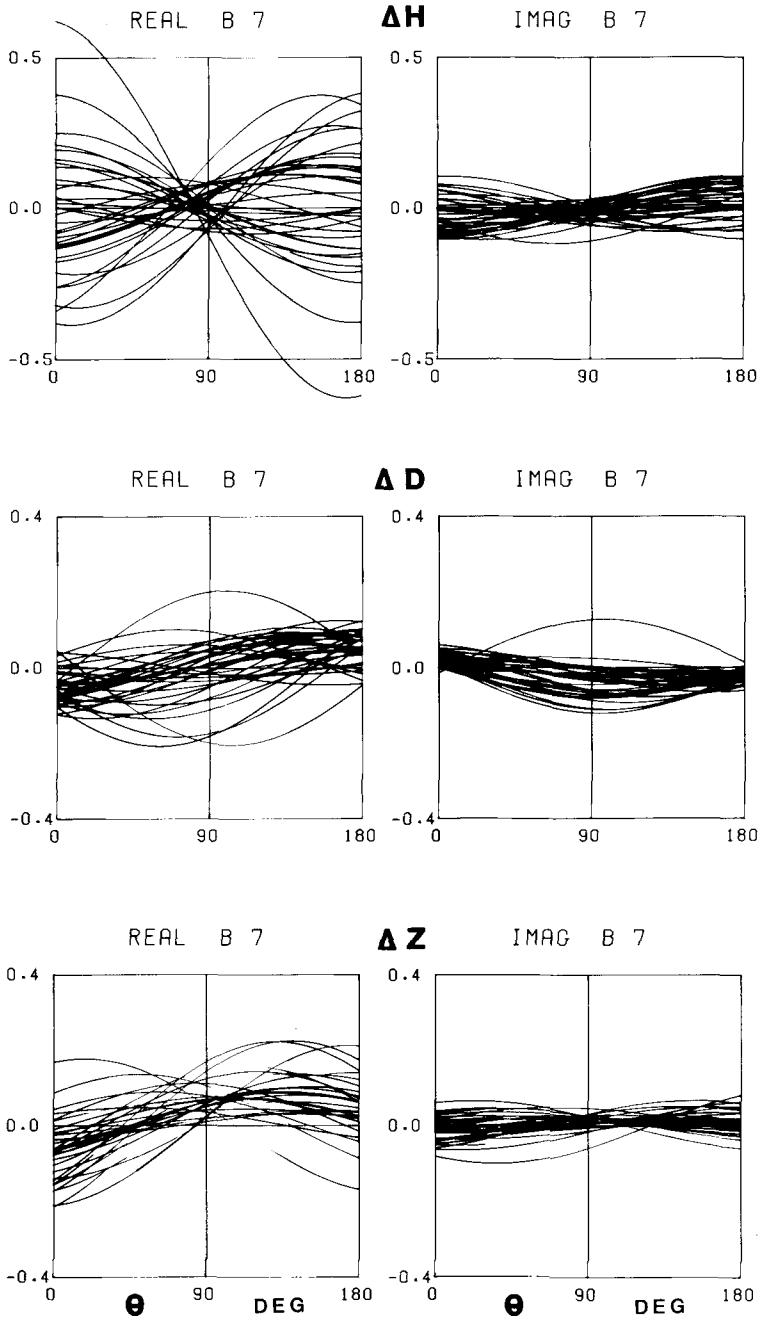

(a)

Figure 8. The real and imaginary parts of the ΔH, ΔD and ΔZ transfer functions, plotted as a function of reference horizontal field azimuth (θ), for all array sites. (a) BAND 7, (b) BAND 15.

azimuth θ $(0 < \theta < 180^\circ)$ at all the array sites, for BAND 7. The corresponding behaviour for BAND 15 is shown in Fig. 8(b). It is evident from these plots that in order to maximize the anomalous fields across the array a suitable choice is $\theta = 0^\circ$ for ΔH and ΔZ while the ΔD component requires $\theta = 90^\circ$. This choice of azimuth is made in the first instance; other criteria concerning the choice of azimuth can be evaluated at a later stage.

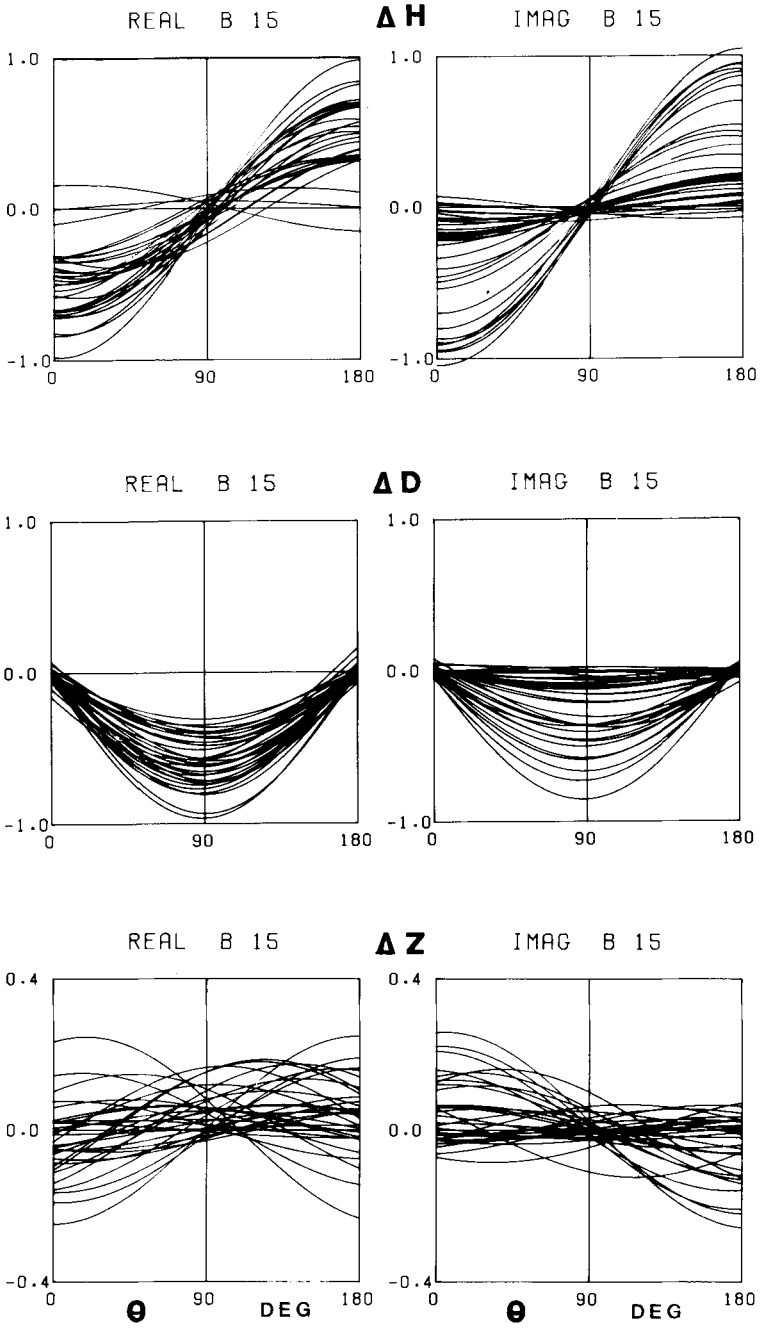

(b)

In the case of the ΔH field, we chose $\theta = 0°$. The ΔH field mapped across the array for BAND 7 is shown in Figs 9(a) (real part) and 9(b) (imaginary part). An anomalous ΔH field represents only the effects of E–W current flow and provides no information about the N–S component. It is evident that the largest fields generated are in-phase with the regional horizontal field, although the imaginary part is significant. Over a large part of the array, the magnitude of $|\Delta H|$ is less than 25 per cent of the reference horizontal field,

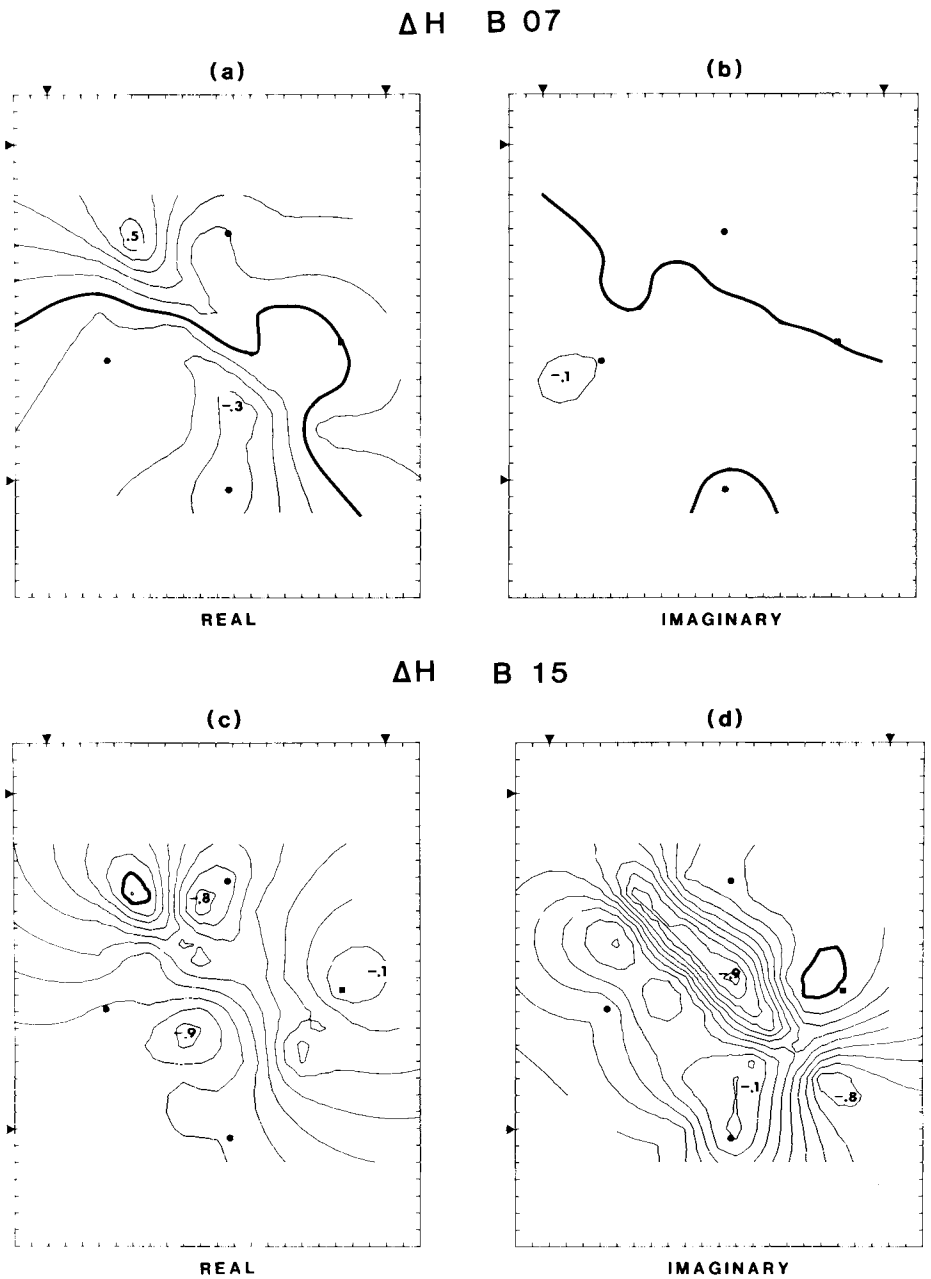

Figure 9. Contour maps of the real and imaginary parts of the ΔH field across the array, when the reference field azimuth $\theta = 0°$. (a) BAND 7, real. (b) BAND 7, imaginary. (c) BAND 15, real. (d) BAND 15, imaginary.

however a much larger variation occurs in the NW corner of the region. The ΔH field mapped across the array for BAND 15 is shown in Figs 9(c) (real part) and 9(d) (imaginary part). It is evident that at this shorter period, the magnitude of both the real and imaginary parts of ΔH can approach the same order as the reference horizontal field. The real part of ΔH shows a general correspondence to that obtained for BAND 7 (Fig. 9a) with the anomaly in the NW corner of the region having intensified. The imaginary part of the ΔH

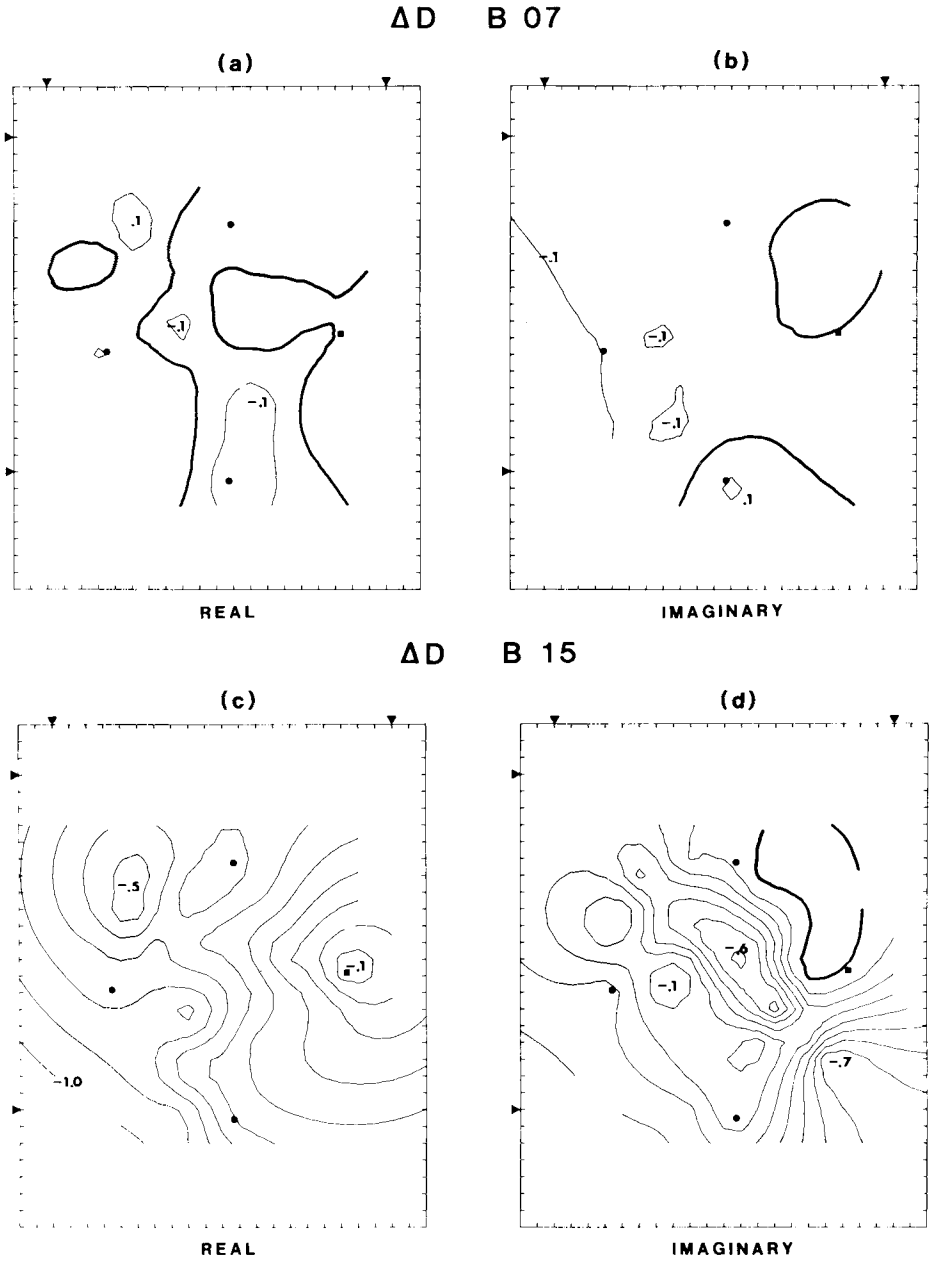

Figure 10. Contour maps of the real and imaginary parts of the ΔD field across the array, when the reference field azimuth $\theta = 90°$. (a) BAND 7, real. (b) BAND 7, imaginary. (c) BAND 15, real. (d) BAND 15, imaginary.

field for BAND 15 is substantial and strongly contrasts with the equivalent map obtained for BAND 7. The map shown in Fig. 9(d) defines, what appears to be, a NW–SE-trending and isolated anomaly across the array region.

In the case of the ΔD field, we choose $\theta = 90°$. The ΔD field mapped across the array for BAND 7 is shown in Figs 10(a) (real part) and 10(b) (imaginary part). An anomalous ΔD field represents only the effects of N–S current flow and provides no information about the E–W component. It is evident that both real and imaginary parts of ΔD are small and as such do not delineate any appreciable structure due to N–S current flow across the region. The ΔD field mapped across the array for BAND 15 is shown in Figs 10(c) (real part) and 10(d) (imaginary part). Both real and imaginary parts of the ΔD field may be compared with the equivalent ΔH field (Fig. 9c, d). Although reduced with respect to the ΔH field, they are found to delineate the same anomalous features.

It is worth remarking that the information provided by the ΔH and ΔD maps is essentially the same as that derived from a differential GDS experiment (Babour & Mosnier 1977; Beamish 1983). We feel, however, that the attributes of the present analysis (dependence of the fields on frequency and horizontal field azimuth) provide a more sophisticated technique for interpretation. It is apparent from the results presented that for BAND 7 the anomalous horizontal fields are largely due to E–W current flow. Values in the ΔH map increase positively to the north over the Northumberland basin. The largest anomaly occurs at the site furthest into the basin. A very clear NW–SE-trending anomaly is observed in the ΔH map. In BAND 15 both E–W and N–S current flow contribute to the anomalous horizontal fields. Equivalent anomalous features across the region are delineated by the ΔH and ΔD maps. At this period, the real and imaginary part of the fields, both of which are substantial, can be used separately to define different structural features of the region.

We next consider the three estimates of the anomalous vertical field denoted T, S and ΔZ which, using HEA, may be used to predict the anomalous vertical field across the array. We

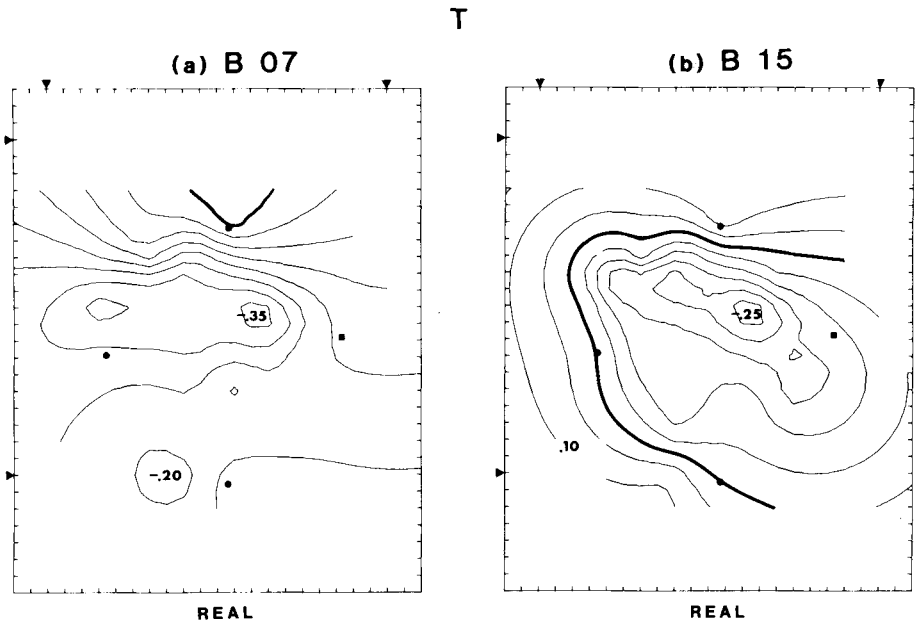

Figure 11. Contour maps of the real part of the anomalous vertical field across the array, using the T transfer functions, when the reference horizontal field azimuth $\theta = 0°$. (a) BAND 7. (b) BAND 15.

choose the azimuth $\theta = 0°$, which corresponds to E–W current flow, for all three predictions. We might assume in each case that the maps are the vertical fields of the anomalous internal currents which flow when the normal horizontal magnetic field across the area has unit amplitude and is directed north. Clearly our predictions are only estimates of this process. We first consider the vertical field map obtained for T. The T field mapped across the array for BAND 7 is shown in Fig. 11(a) (real part). We observe a steep belt of gradients in the north corresponding to anomalous E–W currents associated with the southern margin of the Northumberland basin and linking the North and Irish seas. The T field mapped across the array for BAND 15 is shown in Fig. 11(b) (real part). We now observe a second belt of gradients trending N–S along the western margin of the Alston Block. These results are now compared with the equivalent maps obtained from the transfer functions denoted by S. The real parts of the S fields mapped across the array for BANDS 7 and 15 are shown in Figs 12(a) and (b) respectively. Comparing the results obtained for BAND 7 (Fig. 11a, b) we observe what amount to second-order differences between the two predictions. In particular the S map indicates a WNW–ESE structure (*cf.* E–W) in the north and gradients in the south are only defined by the S map. Comparing the results obtained for BAND 15, we observe what amounts to first-order differences between the two predictions. The N–S-trending belt of gradients in the west which appear on the T map (Fig. 11b) are not apparent on the corresponding S map (Fig. 12b). Other significant differences are observed in the NW part of the region. We note that the T maps ignore the spatial variation in the anomalous horizontal fields across the array and as such the maps do not provide a correct physical basis for interpretation. The anomalous horizontal fields ΔH and ΔD have been mapped in Figs 9 and 10 and it is apparent that they can account for the first- and second-order differences between the T and S field predictions for BANDS 15 and 7. The prediction of the anomalous vertical field by the S map does, however, provide a consistent

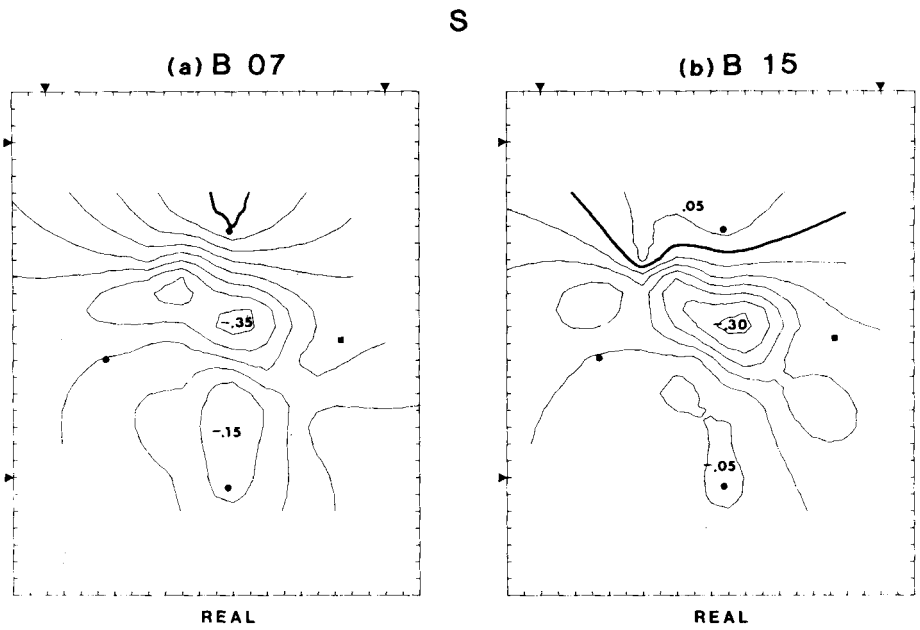

Figure 12. Contour maps of the real parts of the anomalous vertical field across the array, using the S transfer functions, when the reference horizontal field azimuth $\theta = 0°$. (a) BAND 7. (b) BAND 15.

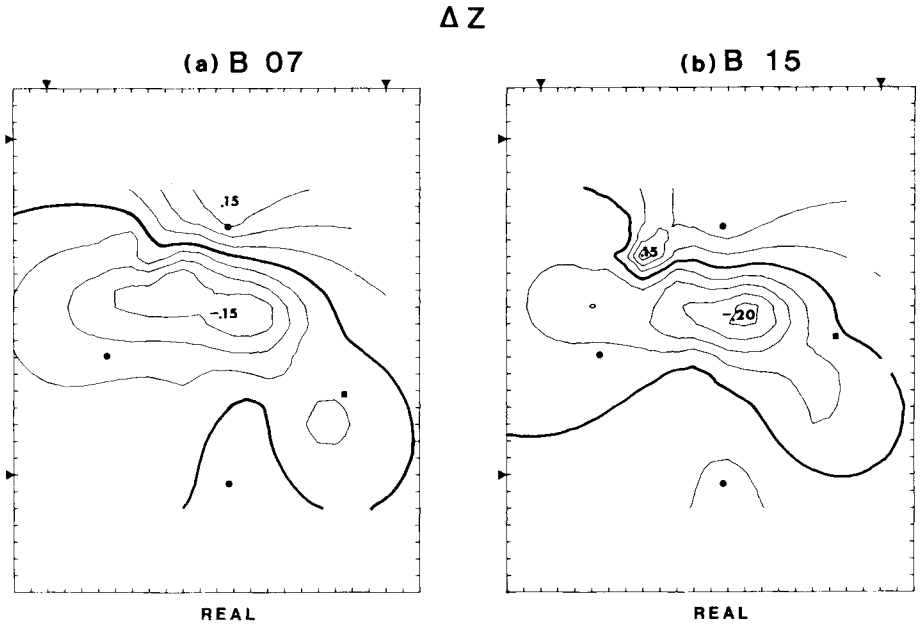

Figure 13. Contour maps of the real parts of the anomalous vertical field across the array, using the ΔZ transfer functions, when the reference horizontal field azimuth $\theta = 0°$. (a) BAND 7. (b) BAND 15.

physical basis for interpretation in that it does predict the anomalous vertical field across the array in response to a specified horizontal field at the reference site.

We cannot apply HEA to the difference field estimates of the anomalous vertical field (ΔZ) in order to predict the anomalous vertical field as indicated above. A simple basis for interpretation would only be provided if the reference site were normal. We can, however, apply HEA to the ΔZ estimates to provide a useful *indicator* of anomalous structure. The ΔZ fields mapped across the array for BANDS 7 and 15 are shown in Figs 13(a) and (b), respectively. A comparison of these maps with the equivalent maps obtained from the S prediction reveals that, although the field values differ, the same anomalous structure is defined in both cases.

Limitations of the method

The transfer functions obtained by common reference processing provide a uniform transfer function data set at each array site. The uniformity of the data set is provided by the fact that all anomalous field components, denoted ΔH, ΔD, ΔZ (and S) are related to the horizontal fields recorded at the reference site. Such a uniform set of transfer functions can be used to predict and map the three estimated anomalous field components associated with a particular horizontal field at the reference site. The limitations of the method lie in the fact that the reference field is not a normal field and hence the contribution of the anomalous horizontal fields at the reference site to the transfer functions obtained across the array remains undefined. The limitations of the method may be investigated by assuming that data (H_n, D_n, Z_n) were obtained from a hypothetical normal site in conjunction with the data obtained at the reference site (H_r, D_r, Z_r). At all non-normal sites we may write the total observed fields as the sum of normal (n) and anomalous (a) parts, i.e. $H_i = H_n + H_{ai}$, $D_i = D_n + D_{ai}$, $Z_i = Z_n + Z_{ai}$.

The estimate of the anomalous field is obtained from (3)–(5) as:

$$H_i - H_r = H_{ai} - H_{ar} = h_{Hi} \cdot H_r + h_{Di} \cdot D_r \tag{10}$$

$$D_i - D_r = D_{ai} - D_{ar} = d_{Hi} \cdot H_r + d_{Di} \cdot D_r \tag{11}$$

$$Z_i - Z_r = Z_{ai} - Z_{ar} = z_{Hi} \cdot H_r + z_{Di} \cdot D_r \tag{12}$$

where we assume noise-free fields. We now use the normal field components as a second reference to obtain equivalent transfer functions between the reference and normal sites:

$$H_r - H_n = H_{ar} = h_{Hr} \cdot H_n + h_{Dr} \cdot D_n \tag{13}$$

$$D_r - D_n = D_{ar} = d_{Hr} \cdot H_n + d_{Dr} \cdot D_n \tag{14}$$

$$Z_r - Z_n = Z_{ar} = z_{Hr} \cdot H_n + z_{Dr} \cdot D_n \tag{15}$$

where the transfer functions defined by (13)–(15) are unknown. Equations (10)–(12) and (13)–(15) can be used to obtain expressions between the anomalous field components (H_{ai}, D_{ai}, Z_{ai}) at each site and the normal field components (H_n, D_n, 0). Rewriting the estimated transfer functions in equations (10)–(12) as:

$$W_{1i} = t_{Hi} + z_{Hi} = s_{Hi}$$

$$W_{2i} = t_{Di} + z_{Di} = s_{Di}$$

$$W_{3i} = h_{Hi}$$

$$W_{4i} = h_{Di}$$

$$W_{5i} = d_{Hi}$$

$$W_{6i} = d_{Di}$$

where we have used the previously noted identities between the transfer function estimates of equations (2) and (9), we obtain, after some manipulation:

$$H_{ai} = [W_{3i} + (1 + W_{3i}) \cdot h_{Hr} + W_{4i} \cdot d_{Hr}] \cdot H_n + [W_{4i} + (1 + W_{3i}) \cdot h_{Dr} + W_{4i} \cdot d_{Dr}] \cdot D_n \tag{16}$$

$$D_{ai} = [W_{5i} + W_{5i} \cdot h_{Hr} + (1 + W_{6i}) \cdot d_{Hr}] \cdot H_n + [W_{6i} + W_{5i} \cdot h_{Dr} + (1 + W_{6i}) \cdot d_{Dr}] \cdot D_n \tag{17}$$

$$Z_{ai} = [W_{1i} + W_{1i} \cdot h_{Hr} + W_{2i} \cdot d_{Hr}] \cdot H_n + [W_{2i} + W_{1i} \cdot h_{Dr} + W_{2i} d_{Dr}] \cdot D_n \tag{18}$$

as predictive equations for the anomalous field components.

The four complex unknowns are the transfer functions relating the anomalous horizontal fields at the reference site to the horizontal fields at a normal site. If the reference site were normal, the unknown transfer functions would be zero and the predictive equations would be:

$$H_{ai} = W_{3i} \cdot H_r + W_{4i} \cdot D_r \tag{19}$$

$$D_{ai} = W_{5i} \cdot H_r + W_{6i} \cdot D_r \tag{20}$$

$$Z_{ai} = W_{1i} \cdot H_r + W_{2i} \cdot D_r . \tag{21}$$

Because the reference site is not normal, a prediction made in this way will not give the

correct anomalous fields. Instead the predictions obtained, on substituting for H_r, D_r, will be:

$$H'_{ai} = (W_{3i} + W_{3i} \cdot h_{Hr} + W_{4i} \cdot d_{Hr}) \cdot H_n + (W_{4i} + W_{3i} \cdot h_{Dr} + W_{4i} \cdot d_{Dr}) \cdot D_n \quad (22)$$

$$D'_{ai} = (W_{5i} + W_{5i} \cdot h_{Hr} + W_{6i} \cdot d_{Hr}) \cdot H_n + (W_{6i} + W_{5i} \cdot h_{Dr} + W_{6i} \cdot d_{Dr}) \cdot D_n \quad (23)$$

$$Z'_{ai} = (W_{1i} + W_{1i} \cdot h_{Hr} + W_{2i} \cdot d_{Hr}) \cdot H_n + (W_{2i} + W_{1i} \cdot h_{Dr} + W_{2i} \cdot d_{Dr}) \cdot D_n. \quad (24)$$

On comparing equations (22) and (16), (23) and (17), (24) and (18) we obtain the errors obtained in our predictions as:

$$\delta H_i = h_{Hr} \cdot H_n + h_{Dr} \cdot D_n \quad (25)$$

$$\delta D_i = d_{Hr} \cdot H_n + d_{Dr} \cdot D_n \quad (26)$$

$$\delta Z_i = 0. \quad (27)$$

From this last result, it would appear that we can always predict the anomalous vertical field accurately although the anomalous horizontal fields that we predict will be biased by the presence of anomalous horizontal fields at the reference site. We note, however, that if the transfer functions h_{Hr}, h_{Dr}, d_{Hr} and d_{Dr} remain undefined, the relationship between the azimuth and phase of the specified horizontal field at the reference site (i.e. the input to our predictive equations) to that of the corresponding normal horizontal field also remains undefined.

Having noted the limitations of the transfer functions provided by the method it appears possible, in theory, to apply a further constraint to our predictions of the anomalous field components. Equations (22)–(24) provide estimates of the three anomalous field components but the equations contain four unknown transfer functions. We know, from potential theory, that the anomalous field components must be mutually consistent, in that, they must be expressible as the gradient of a potential function (Weaver 1963, and references therein). This constraint allows separation formulae between internal and external field components to be derived. In addition, for general, three-dimensional fields, three relationships must exist between the Fourier transforms of the anomalous (internal) field components (Weaver 1963, equations 22, 23 and 25). It is thus possible, in theory, to apply such a constraint to the three anomalous field components generated using equations (22)–(24), and to solve for the four unknown transfer functions in a least-squares sense. Such a procedure could, therefore, provide an optimum description of the anomalous field components across the array, consistent with the transfer function estimates, their errors and the constraints provided by potential theory. Work on this aspect of the problem is currently in progress.

Conclusions

In this experiment, a technique has been employed that utilizes a reference magnetometer together with a small number of field magnetometers. The technique enables regional array data to be collected using a modest amount of field equipment. The three anomalous field components at each array site are estimated by transfer functions obtained using common reference processing. A uniformity exists in the transfer function estimates obtained since

they are all related to the horizontal field components at the reference site. Maps of the anomalous field components may be generated by using the transfer function estimates to predict the three anomalous field components associated with a specified horizontal field at the reference site. The procedure makes no assumptions concerning the nature of the induced currents responsible for the observed anomalous fields. The nature of such currents should, in fact, be deduced from the results obtained.

The limitation of the method lies in the bias error introduced into the transfer function estimates by anomalous horizontal fields at the reference site. We find that such an error only exists in the estimates of the anomalous horizontal fields and does not affect the estimates of the anomalous vertical field. Such a limitation does *not* affect the mapping of anomalous structures using hypothetical event analysis because the correct spatial variation of the three anomalous field components across the array is accurately predicted. The bias error is only a problem when regional boundary conditions need to be specified. Ideally, these should be specified in terms of a normal horizontal field. This can only be achieved if four unknown transfer functions relating the anomalous horizontal fields at the reference site to normal horizontal fields can be determined.

It has been possible using the array data obtained to compare two different estimators of the anomalous vertical field. The more common single-site vertical field transfer function requires uniform horizontal fields across the array region to provide an accurate spatial map. The vertical field transfer function obtained using common reference processing is accurate irrespective of the horizontal field variation across the region. The predicted anomalous vertical fields using the two estimators have been presented and compared for two period ranges and the first- and second-order differences have been noted. The observed differences can be accounted for by the observed variation in horizontal field components across the array.

The data for this experiment were obtained from a region of northern England whose crustal structure can be considered well-defined. It has been argued on the basis of the frequency dependence of the estimated anomalous field that two modes of induced current flow can be identified at periods less than 2000 s. The two systems of induced current flow produce peaks in the anomalous vertical field at long (around 1000 s) and short (around 60 s) periods. The two systems of induced current can equally well be identified from the frequency dependence of the anomalous horizontal fields.

The nature of the induced current system flowing across the region can be further deduced from the observed spatial variation of the anomalous field components across the array. At long periods (around 1000 s), a regional E-polarization mode is defined by E–W current flow which appears concentrated along the southern margin of the Northumberland Trough. This current system produces a large-scale regional variation in Z_a (Fig. 12a) and smaller-scale variations in H_a (Fig. 9a). The anomalous fields are largely, but by no means entirely, in-phase with the reference horizontal fields. We interpret this induced current system as part of a thin-sheet induction process involving the shelf seas and major sedimentary basins (see also Banks, Beamish & Geake 1983). It is evident from the observed spatial variations in the anomalous field components at short periods (around 60 s), that the anomalous fields in-phase with the reference horizontal fields (Figs 9c and 12b) are still in-part derived from an E–W current system associated with the southern margin of the Northumberland Trough. Additional large- and small-scale anomalous features are, however, well resolved by the results obtained. It is apparent from Figs 9(d) and 10(d) that the largest anomalous horizontal fields generated at short periods are in-quadrature with the reference horizontal fields and define a consistent anomaly pattern that is independent of E–W current flow within the sedimentary basins. If we compare the anomalous horizontal field results shown in these two figures with the corresponding result obtained for the in-

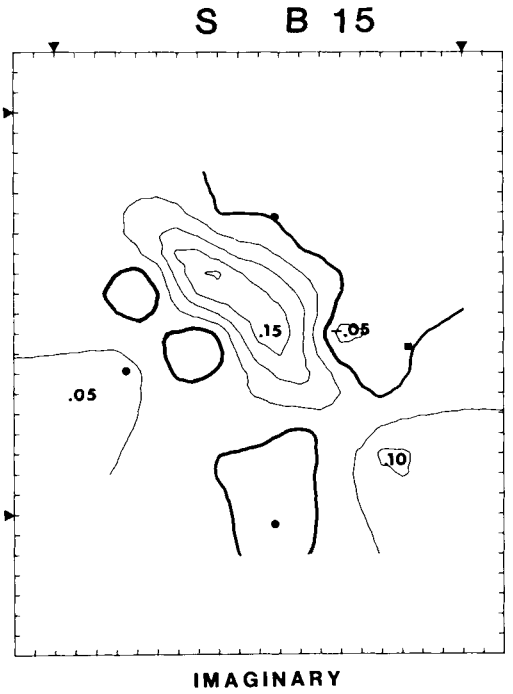

Figure 14. Contour map of the imaginary part of the anomalous vertical field across the array, using the S transfer functions, when the reference horizontal field azimuth $\theta = 0°$. BAND 15.

quadrature (imaginary) part of the anomalous vertical field shown in Fig. 14, we observe a high degree of consistency in the definition of a NW/SE-trending and isolated pattern of anomalous field components across the array region.

If we regard the characteristics of the observed variation fields at long periods as largely determined by the resistive flow of current in a thin sheet, we should correspondingly regard the characteristics observed at short periods as determined by a mode of induced current flow possessing both resistive and reactive characteristics. It is in this respect that the anomalous fields at short periods appear to define a local induction process in the isolated conducting structures across the region. Such an interpretation of the results has an obvious implication with regard to the type of modelling that may be undertaken. In summary, we find that the techniques described appear to have enabled anomalous fields to be defined in an optimum manner across northern England. The information generated has led to some measure of understanding in relation to the prevailing regional nature of the electromagnetic induction process. The maps of anomalous field components have revealed a number of interesting, and indeed surprising, features which are currently the subject of more detailed analysis.

Acknowledgments

We are indebted to the hill farmers and landowners of the northern Pennines who supplied both assistance with and permission for the field experiment. Michael Geake and Dr Roland Roberts ably assisted with the field work. We gratefully acknowledge the support of the Natural Environment Research Council in the form of grant GR3/2371 and a grant from the Deep Geology Project. This paper is published with the approval of the acting Director, Institute of Geological Sciences (NERC).

References

Babour, K. & Mosnier, J., 1977. Differential geomagnetic sounding, *Geophysics,* **42,** 66–76.

Bailey, R. C., Edwards, R. N., Garland, G. D. Kurtz, R. & Pitcher, D., 1974. Electrical conductivity studies over a tectonically active area in eastern Canada, *J. Geomagn. Geoelect., Kyoto,* **26,** 125–146.

Banks, R. J. 1975. Complex demodulation of geomagnetic data and the estimation of transfer functions, *Geophys. J. R. astr. Soc.,* **43,** 87–101.

Banks, R. J., 1981. Strategies for improved global electromagnetic response estimates, *J. Geomagn. Geoelect., Kyoto,* **33,** 569–585.

Banks, R. J. & Beamish, D. 1983. Local and regional induction in the British Isles, *Geophys. J. R. astr. Soc.,* to be submitted.

Banks, R. J., Beamish, D. & Geake, M. J., 1983. Magnetic variation anomalies in northern England and southern Scotland, *Nature,* **303,** 516–518.

Beamish, D., 1977. The mapping of induced currents around the Kenya Rift: a comparison of techniques, *Geophys. J. R. astr. Soc.,* **50,** 311–332.

Beamish, D., 1979. Source field effects on transfer functions at mid-latitudes, *Geophys. J. R. astr. Soc.,* **58,** 117–134.

Beamish, D., 1983. A comparison of time and frequency domain geomagnetic sounding, *Geophys. J. R. astr. Soc.,* **73,** 689–704.

Bott, M. H. P., 1967. Geophysical investigations of the northern Penine basement rocks, *Proc. Yorks. geol. Soc.,* **36,** 139–168.

Bott, M. H. P., 1974. The geological interpretation of a gravity survey of the English Lake District and the Vale of Eden, *J. geol. Soc. Lond.,* **130,** 309–331.

Duffus, H. J., Shand, J. A., Wright, C. S., Nasmyth, P. W. & Jacobs, J. A., 1959. Geographical variations in geomagnetic micropulsations, *J. geophys. Res.,* **64,** 581–583.

England, P. C., Oxburgh, E. R. & Richardson, S. W., 1980. Heat refraction and heat production in and around granite plutons in north-east England, *Geophys. J. R. astr. Soc.,* **62,** 439–455.

Everett, J. E. & Hyndman, R. D., 1967. Geomagnetic variations and electrical conductivity structure in south-western Australia, *Phys. Earth planet. Int.,* **1,** 24–34.

Reitzel, J. S., Gough, D. I., Porath, H. & Anderson, C. W., 1970. Geomagnetic deep sounding and upper mantle structure in the western United States, *Geophys. J. R. astr. Soc.,* **19,** 213–235.

Richardson, S. W. & Oxburgh, E. R., 1979. The heat flow field in mainland UK, *Nature,* **282,** 565–567.

Schmucker, U., 1964. Anomalies of geomagnetic variations in the southwestern United States, *J. Geomagn. Geoelect., Kyoto,* **15,** 193–221.

Schmucker, U., 1970. Anomalies of geomagnetic variations in the southwestern United States, *Bull. Scripps Inst. Oceanogr.,* **13,** University of California Press, 165 pp.

Schmucker, U., 1973. Regional induction studies: a review of methods and results, *Phys. Earth planet. Int.,* **7,** 365–378.

Swinburn, P. M., 1975. The crustal structure of northern England, *PhD thesis,* University of Durham.

Weaver, J. T., 1963. On the separation of local geomagnetic fields into external and internal parts, *J. Geophys.,* **30,** 29–36.

White, R. E., 1973. The estimation of signal spectra and related quantities by means of the multiple coherence function, *Geophys. Prosp.,* **21,** 660–703.